LONG BASELINE OBSERVATIONS OF HD100546 WITH ALMA:
A POSSIBLE CIRCUMPLANETARY DISK DETECTED IN DUST CONTINUUM AND GAS KINEMATICS

Sebastián Pérez,[1,2] Simon Casassus,[2] Antonio Hales,[3,4] Sebastián Marino,[5] Anthony Cheetham,[6,5] Alice Zurlo,[7,8] Lucas Cieza,[7] Ruobing Dong,[9] Felipe Alarcón,[10] Pablo Benítez-Llambay,[11] and Ed Fomalont[3,4]

[1]Universidad de Santiago de Chile, Av. Libertador Bernardo O'Higgins 3363, Estación Central, Santiago, Chile

[2]Departamento de Astronomía, Universidad de Chile, Casilla 36-D, Santiago

[3]National Radio Astronomy Observatory, 520 Edgemont Road, Charlottesville, VA 22903-2475, USA

[4]Atacama Large Millimeter/Submillimeter Array, Joint ALMA Observatory, Alonso de Córdova 3107, Vitacura 763-0355, Santiago, Chile

[5]Max Planck Institute for Astronomy (MPIA), Königstuhl 17, 69117 Heidelberg, Germany

[6]Observatoire de Genve, Universit de Genve, 51 chemin des Maillettes, 1290, Versoix, Switzerland

[7]Universidad Diego Portales, Av. Ejercito 441, Santiago, Chile

[8]Escuela de Ingeniería Industrial, Facultad de Ingeniería y Ciencias, Universidad Diego Portales, Av. Ejercito 441, Santiago, Chile

[9]Department of Physics & Astronomy, University of Victoria, Victoria, BC, V8P 1A1

[10]Department of Astronomy, University of Michigan, 1085 S. University, Ann Arbor, MI 48109, USA

[11]Niels Bohr International Academy, Niels Bohr Institute, Blegdamsvej 17, DK-2100 Copenhagen Ø, Denmark

ABSTRACT

Giant planets growing in a circumstellar disk interact dynamically with the whole disk, and planetary growth is thought to be regulated by the circumplanetary disk (CPD) and its immediate environment. How much dust is gathered in the CPD, in addition to the gas, is a standing question in planet formation theories. Using the Atacama Large Millimeter/submillimeter Array, we observed the star HD 100546, host to a prominent disk with a deep, wide gap. Here, we report a 6σ detection of a point source of 1.3 mm continuum emission which lies in the middle of this wide gap. The lack of any signal in SPHERE sparse aperture masking data discards a stellar origin. The 6σ signal is located 51 milli-arcsecond away from the central star, at a position angle of $37°$, as of September 2017. If in a co-planar configuration with the disk, the point source is at a deprojected separation of 7.8 au on a 16 yr orbit, comparable to Jupiter's orbit. This discovery is supported by the CO gas kinematics of the cavity whose velocity map is distorted at the source location. The mm flux, the distorted kinematics, and the upper limit on the size of the emitting region are compatible with circumplanetary disk emission. In addition to the signatures inside the gap, a strong signpost of disk-planet interaction is also found at $0.''25$ to the north west, adjacent to the continuum ring.

1. INTRODUCTION

Simulations of planet-disk interaction show that young massive planets develop a *circumplanetary disk* (CPD) as they accrete material from their parent protoplanetary disk (e.g., Miki 1982; Lubow et al. 1999; Gressel et al. 2013; Szulágyi et al. 2014). The CPDs persist for as long as the planet grows. CPDs, however, have eluded detection in dust continuum (Wu et al. 2017; Ricci et al. 2017) even in long, deep observations (Isella et al. 2014). Indeed, the radio flux emitted by these CPDs may be scarce because millimeter dust

Corresponding author: Sebastián Pérez
sebastian.astrophysics@gmail.com

is believed to be lost by radial drift within a few hundred years (Zhu et al. 2018). But, how much dust is collected in the circumplanetary vicinity? is this material enough to form satellites? is it replenished? The detection of a protoplanet, via its CPD dust continuum and gas kinematics, would help answering these questions.

From high-contrast direct imaging at infrared and optical wavelengths, a handful of protoplanetary disks have been reported to host candidate CPD detections: HD 100546 (Quanz et al. 2013a, 2015; Brittain et al. 2014; Currie et al. 2015), LkCa15 (Kraus & Ireland 2012; Sallum et al. 2015), HD 169142 (Quanz et al. 2013b; Biller et al. 2014; Reggiani et al. 2014), and MWC 758 (Reggiani et al. 2018). These detections have been challenged as they could represent resid-

ual disk features (Thalmann et al. 2016; Follette et al. 2017; Sissa et al. 2018), especially when angular differential imaging (ADI) post-processing is applied (Rameau et al. 2017; Ligi et al. 2018), or be the product of shock heating due to unseen protoplanets or spirals (Hord et al. 2017). Detections in Hα emission, which is thought to be an accretion tracer (Aoyama et al. 2018), have been questioned as filtered extended emission (Mendigutía et al. 2018). The protoplanet candidate inside the gap of PDS 70 is the only detection still standing (Keppler et al. 2018). Recently, evidence for a CPD as an infrared excess on the spectrum of PDS 70b has been presented by Christiaens et al. (2019a), using the AN-DROMEDA spectral extraction algorithm Cantalloube et al. (2015). Although the biases involved in ANDROMEDA have not been quantified, the resulting spectrum is similar to that obtained by Christiaens et al. (2019b) after extensive assessment of biases. However, so far it has not been possible to image the concomitant circumplanetary disks directly in millimeter emission for any of these protoplanets (Isella et al. 2014; Keppler et al. 2019).

In Perez et al. (2015), we show that a CPD embedded in a circumstellar disk produces distinct kinematical signatures, detectable in CO velocity maps when probed at high resolution and sensitivity. One of the predicted characteristics of a CPD is a kink or wiggle in the iso-velocity contours of CO emission in the vicinity of the CPD. Pinte et al. (2018) observed such a kink in iso-velocity maps of HD 163296, identifying the presence of a giant planet at 260 au.

In this Letter, we present 1.3 mm observations of HD 100546 at ≤2 au resolution (Section 2). Inside the gap, a point source of continuum emission is detected at 6σ (Section 3). The gas kinematics in the vicinity of this point source bears similarities with those expected for circumplanetary material around an accreting giant. Infrared observations (Section 3.1) rule out the presence of stellar companions inside the gap. A second kinematic detection outside the continuum ring is presented in Section 4 and in a companion Letter (Casassus & Pérez 2019). The nature of the continuum point source, as well as the kinematic signatures present in HD 100546, are discussed in Section 5.

2. OBSERVATIONS

We obtained 1.3 millimeter observations of HD 100546 by combining ALMA 12-m array extended (C40-9) and more compact (C40-6) configurations, in the context of Cycle 4 project 2016.1.00344.S, resulting in baselines ranging from 19 meters to up to 12.2 kilometers and a total of 39-42 antennas. The combined observations are sensitive to spatial scales of up to 1″.5, with a spatial resolution of ∼20 mas (for Briggs weighting with a robust parameter of 0.5). The long baseline observations were acquired on September 19, 22, and 23, in three different blocks of ∼90 min each (40 min on source). Precipitable water vapor ranged between 0.3 and 0.8 mm. Observations of atmospheric (J1147-6753), bandpass (J0635-7516), and flux (J1107-4449) calibrators were performed. The phase calibrator (J1147-6753) was alternated with the science target to calibrate the time-dependent vari-

ation of the complex gains. The cycling time for phase calibration was set to 8 minutes and 54 seconds for the compact and extended configurations, respectively. The ALMA correlator was configured in Frequency Division Mode (FDM). Two spectral windows with 1.875 GHz bandwidth were set up for detecting the dust continuum, centered at 232.005 GHz and 218.505 GHz, respectively. The ^{12}CO(2–1), ^{13}CO(2–1) and C^{18}O(2–1) transitions of carbon monoxide were targeted by configuring three spectral windows at rest frequencies of 230.538 GHz, 220.399 GHz and 219.560 GHz respectively. The spectral resolution for the line observations was 122.070 kHz (equivalent to 0.2 km s^{-1} channels).

All data were calibrated by the ALMA staff using the ALMA Pipeline version 40896 in the CASA package (McMullin et al. 2007), including offline Water Vapor Radiometer (WVR) calibration, system temperature correction, as well as bandpass, phase, and amplitude calibrations. The short baseline and long baseline datasets were calibrated independently.

Synthesis imaging was initially performed using the CLEAN algorithm (CASA version 5.4, task `tclean`). Self-calibration of the data was performed to improve coherence. A positional offset between short and long baseline was corrected prior to combining the datasets. An image reconstructed using natural weights, after self-calibration and concatenation of the datasets, yields an RMS noise of 12μJy beam^{-1}, for a CLEAN beam of 64×45 mas.

As HD 100546 is bright in the mm, we super-resolved the self-calibrated continuum data using non-parametric image modeling with the UVMEM package (here we used the publicly-available GPU adaptation GPUVMEM[1] Cárcamo et al. 2018). Image positivity provided enough regularization (i.e. we did not add entropy to the objective function). The `uvmem` reconstruction $I_{1.3mm}$ provides slightly higher angular resolutions than super-uniform weighting, but without compromising sensitivity. We adopted the `uvmem` image for our analysis.

The final $I_{1.3mm}$ image has an approximate angular resolution of $\Omega_b = 17 \times 11$ mas, as measured on the point source inside the gap. This effective beam is consistent with the expectation of $\lesssim 1/3$ the natural beams (Cárcamo et al. 2018), which is $\Omega_{nat} = 64 \times 45$ mas. We oversample Ω_b with 2.5 mas pixels. The peak in flux is 0.92 mJy beam^{-1}, at the location of the star. The flux density of the central source is 3.1±0.3 mJy, while the total flux density over the entire image is 436±40 mJy.

The following conservative approach was used to assess the noise level in $I_{1.3mm}$. We first measured the noise in the restored image (comparable to a CLEAN restoration), in natural weights. This was done by calculating the standard deviation inside small boxes devoid of bright continuum emission, but including synthesis imaging artifacts. This measurement was repeated over several regions, and the largest standard deviation was adopted as systematic noise. This

---

[1] https://github.com/miguelcarcamov/gpuvmem.
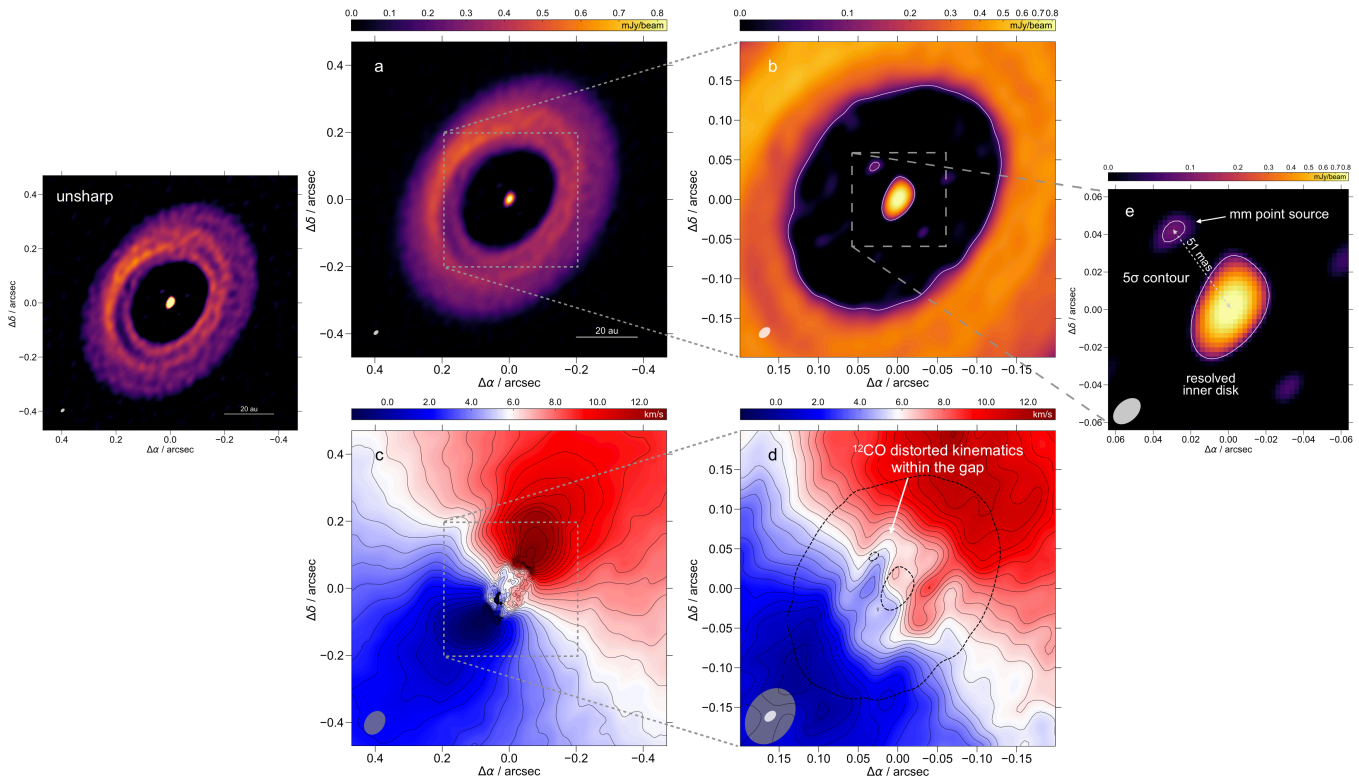
Figure 1. ALMA observations of HD 100546 acquired in September 2017. (a) Dust continuum emission map at 1.3 mm ($I_{1.3\text{mm}}$). (b) Zoomed in view inside the dust gap stretching the color scale using an arcsinh function. Contour level is 5σ. (c) Velocity map (1st moment) from ^{12}CO emission. (d) Zoomed in velocity field inside the dust gap which shows a perturbed non-Keplerian morphology at the radius of the continuum point source. The 5σ continuum level is overlaid with a dashed black contour. (e) shows a close up view of the 1.3 mm continuum map. The left-most panel labelled "unsharp" shows an unsharp-masking version of image (a), to enhance the fine structure of the continuum.

amounts to $\sigma_{\text{natural}} = 56$ μJy beam^{-1}, in the Ω_{nat} beam. Second, we assumed that the noise in $I_{1.3\text{mm}}$ was worse by a factor of $\sqrt{N_b}$, where $N_b \sim 9 = \Omega_b/\Omega_{\text{nat}}$ is the number of `uvmem` beams inside the natural-weight beams. The resulting noise level in $I_{1.3\text{mm}}$ is $\sigma_{\text{MEM}} = 13.2$ μJy beam^{-1}, in the Ω_b `uvmem` beam.

Channel maps of ^{12}CO emission were constructed with `tclean`, on the continuum-subtracted data (continuum subtraction performed with CASA task `uvcontsub`). We used a Briggs weighting scheme with a robust parameter of 1.0, which yield the best results in terms of achieving good signal-to-noise without compromising on resolution. Channel maps were produced with a spectral resolution of 0.5 km s^{-1}. Each channel map has an RMS noise of 1.2 mJy beam^{-1}, for a CLEAN beam of $0\rlap{.}''076 \times 0\rlap{.}''057$.

The ALMA observations of HD 100546 are summarized in Figure 1. The first panel (a) reveals a bright ring in continuum emission (the ring has previously been imaged, most recently by Pineda et al. 2019). The ring displays remarkable radial and azimuthal structure. An unsharp-masked version of the image (left panel in Figure 1), reveals intriguing breaks in the arcs conforming the ring, especially at PA = 80°, where the structures split into two branching arms. Such breaks may perhaps correspond to the superposition of optically thick layers. Continuum emission is detected around

the location of the star. The emission is resolved with a radius of $\sim$1.8 au (half the FWHM along its major axis). We interpret this as thermal emission from an inner disk (Figure 1b). Finally, the lower panels in Figure 1 show the velocity maps of ^{12}CO emission calculated using two methods: Gaussian fits to determine the velocity centroid along each pixel (panel c), and an intensity weighted sum along the spectral axis (d). The traditional intensity weighted map in (d) works best at recovering the broad and velocity-structured emission profiles within the gap.

3. POINT SOURCE AND KINEMATICS IN THE GAP

The long baseline ALMA observations presented here were part of a program to reach high enough sensitivities to map the velocity field of HD 100546 at fine angular scales. The deep integrations required to probe the CO kinematics led to the discovery of a continuum point source within the gap (Figure 1b,e). We measure the point source to be at a separation of 51 ± 2 mas, at a position angle of 37 ± 2 degrees East of North. Given the inclination of the disk (we measure an inclination of 45 ± 3 degrees and a PA of 138 ± 3 degrees), and assuming that the point source is aligned with the disk, this translates to a de-projected separation of 71 ± 5 mas. With the new distance estimate for HD 100546 (110.0 ± 0.6 pc, Gaia Collaboration et al. 2018, DR2), this is

equivalent to a physical separation of 7.8±0.6 au —i.e. in an orbit that would lie between Jupiter and Saturn in our solar system—, corresponding to orbital timescales of 15.8±1.7 yr given the mass of the central object of 1.9±0.1 $M_\odot$ (Casassus & Pérez 2019) and assuming a Keplerian, circular orbit.

The point source detection has a flux of 92±9μJy. This corresponds to 6σ given the uncertainties in our image (including both, thermal and systematic effects, see Section 2). Assuming optical thinness, standard opacities, and a 40 K dust temperature, the 94 μJy point source translates into a dust mass of $\sim 1 M_{\rm Moon}$. Other compact features are also present inside the gap, but with lower fluxes. The brightest of these other features lies immediately south west of the star, and may correspond to a marginal 3σ detection. Any other signal inside the gap are at 2σ.

The 6σ point source detection coincides with a strong kink in the ^{12}CO velocity map inside the gap (Figure 1d), as expected from planet-disk interaction kinematics (Perez et al. 2015; Pinte et al. 2018). The gas-flow within the gap is highly perturbed at the radius where the continuum point source is located. These deviations are manifested along a broad range of position angles, hinting at large scale planet-disk interaction kinematics at play (Pérez et al. 2018). The point source detected at 1.3 mm could indeed be behind the clearing of the wide gap, and also affecting the shape of the inner disk which shows a shoulder to the north of the star. A comparison with hydrodynamic predictions is being developed and will be presented in a future publication.

Other companion candidates have been reported in HD 100546, but at much larger separations from the star than the continuum point source presented here. Quanz et al. (2013a) present candidate "b" at 0.5", while Currie et al. (2015) identified a weakly-polarized disk feature or candidate "c" (see also Brittain et al. 2014). As mentioned in the introduction, these IR detections are being debated (Thalmann et al. 2016; Follette et al. 2017; Hord et al. 2017; Sissa et al. 2018).

3.1. *Could the continuum point source be a stellar object or a background galaxy?*

To assess whether the mm point source is a stellar object inside the gap, we performed sparse aperture masking (SAM) observations with SPHERE IRDIS and IFS instruments on VLT. The observations were acquired in May 15-16 2018, in the K1K2 band, with 1h integration on HD 100546 plus 1h on calibrators. The data processing follows the same procedure as in Cheetham et al. (2019). The data were cleaned using the SPHERE Data Reduction and Handling (DRH) pipeline (Pavlov et al. 2008), including background subtraction, flat fielding and extraction of the spectral data cube. IRDIS and IFS images are produced using the MIRA package (Thiébaut 2008) applied to the closure phases and visibilities, with a hyperbolic regularization term. The weights in the regularization were varied in order to suppress speckles.

The SAM observations (Figure 2) reveal extended signal (probably scattered light) from the disk, and a protoplanetary gap of smaller radius than the one in mm continuum.

The IRDIS image recovers emission from every PA, while IFS only yields signal from the maximum forward scattering angle (towards the south west). The gap is empty at the achieved contrast level.

At the separation of 50 mas, where the 1.3 mm continuum detection lies, the contrast in magnitude is 6.9. To convert this 5σ contrast in upper limits on the mass of putative companions, we used the BT-Settl models by (Allard et al. 2012), adapted for SPHERE filters. This limit corresponds to a mass of 33 $M_{\rm Jup}$ if we assume the youngest age of 4 Myr for the star, or 71 $M_{\rm Jup}$ for the eldest of 12 Myr. We can exclude the presence of stellar companions around HD 100546.

The density of sub-mm galaxies which are brighter than $\sim 100~\mu$Jy is of the order of 10^3 sources per square degree, which translates to 0.0015 sources per square arcsec (ASPECS ALMA Large Program, González-López, priv. comm.). Thus, the likelihood of finding a sub-mm galaxy within HD 100546's gap is <0.1%. Moreover, the compact continuum detection is unresolved at 0.″017 resolution (ALMA beam's major axis), which is a factor 15 smaller than the typical size of sub-mm galaxies (Simpson et al. 2015). Thus, we conclude that this continuum detection, whithin the gap where we also see distorted kinematics, is not a bright sub-millimeter galaxy.

4. SECOND KINEMATIC SIGNATURES AT 0.″25

The full velocity map is shown in Figure 1c. At separations comparable to the continuum ring radius, the iso-velocity contours in the near side of the disk (south west, bottom right) display a symmetric pattern with respect to the disk minor axis. Interestingly, the pattern becomes highly asymmetrical on the far side (north east, top left), especially immediately outward the peak in the continuum ring, approximately 0.″25 north west of the central star. This pattern can be recognized as 'kinks' directly in the iso-velocity channel maps (Figure 3), most clearly between 4.0 and 8.0 km s^{-1}. As stated above, significant deviations from Keplerian motion can be attributed to planet-disk interactions, via the local flow in a CPD and the planet-launched spiral wakes. However, we note that other effects can also produce such kinks in the iso-velocity contours. For example, an optically thick continuum, such as the one in HD 100546, blocks the CO emission from the back side of the disk, inducing structure in the gas velocity map. If the kinks are indeed due to planet-disk interaction kinematics, the location of the embedded perturber can be identified via a Doppler-flip in molecular line moment 1 maps, after subtraction of the axially symmetric flow, which follows the disk rotation curve. Such dopplerflip is indeed associated to the kinematic signature found at 0.″25 in HD 100546. This analysis is presented in a companion Letter (Casassus & Pérez 2019, ApJL, *submitted*).

5. SUMMARY AND CONCLUSIONS

We detected a compact 1.3 mm continuum dust emission source which lies in the middle of the HD 100546 transition disk cavity, at only 51 mas from the central star. This continuum detection was possible thanks to a deep integration
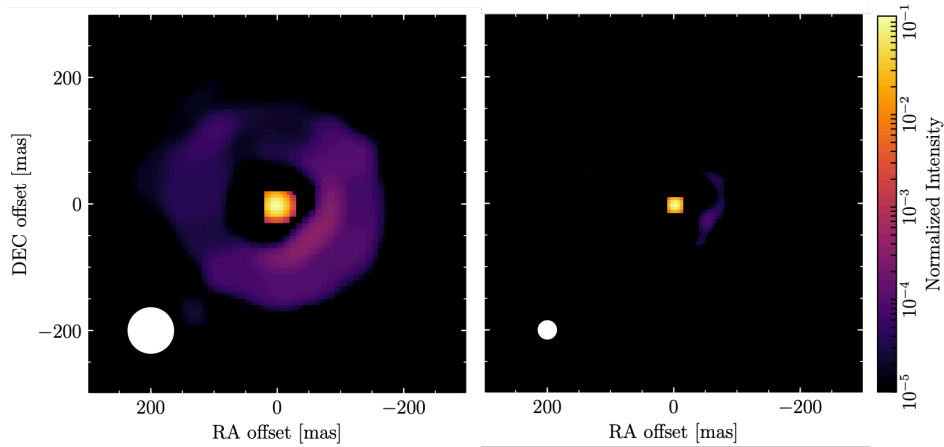
Figure 2. SPHERE SAM observations of HD 100546. The IRDIS (left) and IFS (right) images were produced with the MIRA package, applied to the closure phases and visibilities, with a hyperbolic regularization term. The images show extended scattered light and an empty gap free of stellar companions.

with ALMA at 13 km baselines, aimed at probing for planets in the CO kinematics. The detection is significant at 6σ and its separation from the central star is well resolved by the 17 mas resolution ALMA beam. It is most remarkable that the continuum detection sits in the middle of a wide protoplanetary gap, right under a distorted pattern in the gas kinematics. This type of deviation is expected to be the result of planet-disk interactions. The miniature Keplerian kinematics around the companion, as well as its spiral wakes, affect the line-of-sight velocities in a way that resembles 'kinks' in the iso-velocity contours. This is possibly what happens inside the gap in HD 100546, where both signatures (the mm detection and twisted kinematics) are hard to explain without a companion. A second epoch ALMA observation will not only probe for motion along the 16 yr orbit of the compact dust emission, but will also test if the distorted velocity pattern near the inner disk is constant, as in the case of a warp.

Facilities: ALMA Observatory

Software: GPUVMEM (Cárcamo et al. 2018), CASA (McMullin et al. 2007), MIRA (Thiébaut 2008).

REFERENCES

Allard, F., Homeier, D., & Freytag, B. 2012, Philosophical Transactions of the Royal Society of London Series A, 370, 2765, doi: 10.1098/rsta.2011.0269

Aoyama, Y., Ikoma, M., & Tanigawa, T. 2018, ApJ, 866, 84, doi: 10.3847/1538-4357/aadc11

Biller, B. A., Males, J., Rodigas, T., et al. 2014, ApJ, 792, L22, doi: 10.1088/2041-8205/792/1/L22

Brittain, S. D., Carr, J. S., Najita, J. R., Quanz, S. P., & Meyer, M. R. 2014, ApJ, 791, 136, doi: 10.1088/0004-637X/791/2/136

Cantalloube, F., Mouillet, D., Mugnier, L. M., et al. 2015, A&A, 582, A89, doi: 10.1051/0004-6361/201425571

Cárcamo, M., Román, P. E., Casassus, S., Moral, V., & Rannou, F. R. 2018, Astronomy and Computing, 22, 16, doi: 10.1016/j.ascom.2017.11.003

Casassus, S., & Pérez, S. 2019, submitted to ApJL

Casassus, S., Marino, S., Pérez, S., et al. 2015, ApJ, 811, 92, doi: 10.1088/0004-637X/811/2/92

Cheetham, A. C., Samland, M., Brems, S. S., et al. 2019, A&A, 622, A80, doi: 10.1051/0004-6361/201834112

Christiaens, V., Cantalloube, F., Casassus, S., et al. 2019a, ApJ, 877, L33, doi: 10.3847/2041-8213/ab212b

Christiaens, V., Casassus, S., Absil, O., et al. 2019b, MNRAS, 486, 5819, doi: 10.1093/mnras/stz1232
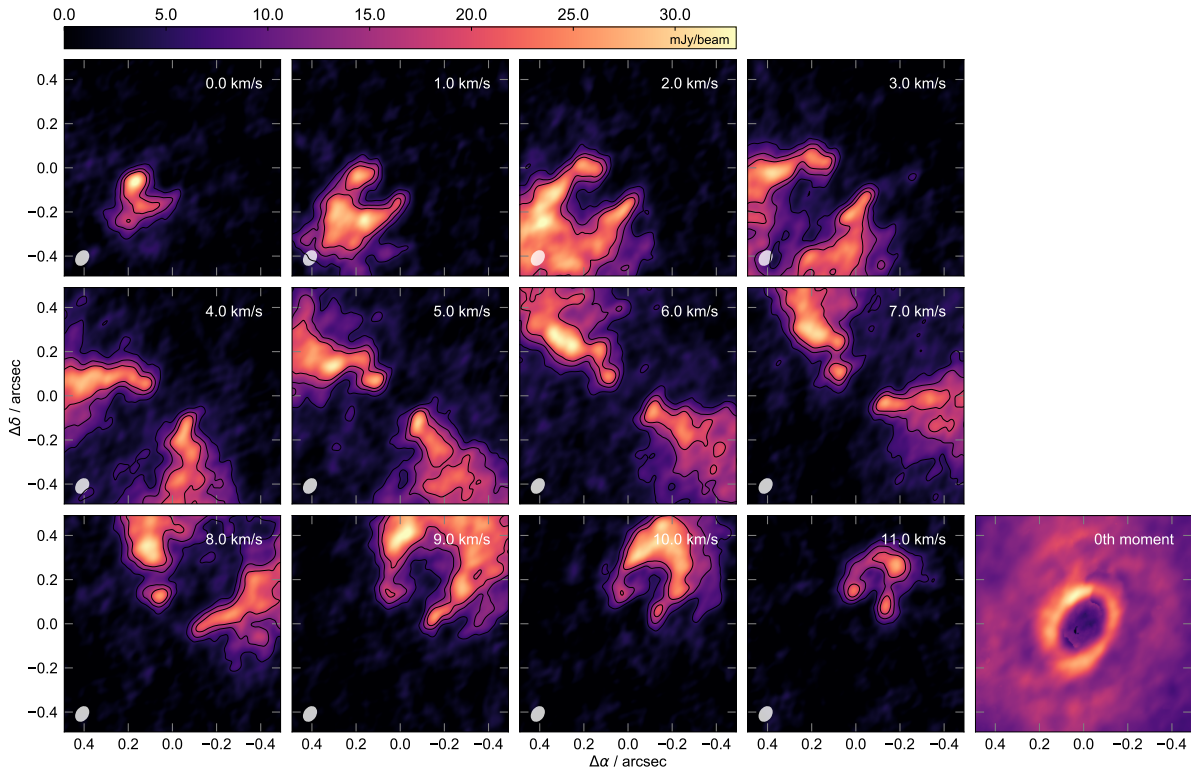
Figure 3. ^{12}CO channel maps of HD 100546 showing several non-Keplerian structures beyond the gap. Most strikingly, it shows velocity 'kinks' along a 0."25 separation north east from the star, covering almost 6 km s^{-1} in velocity. Each panel shows ^{12}CO emission every 1 km s^{-1} (channel widths are 0.5 km s^{-1}). Contours correspond to 5, 10, and 15 times the channel RMS (1.2 mJy beam^{-1}). The synthetized beam of the CLEAN reconstruction is shown in the bottom left corner. The zeroth moment is shown in the last (bottom right) panel.

Close, L. M., Follette, K. B., Males, J. R., et al. 2014, ApJ, 781, L30, doi: 10.1088/2041-8205/781/2/L30

Currie, T., Cloutier, R., Brittain, S., et al. 2015, ApJ, 814, L27, doi: 10.1088/2041-8205/814/2/L27

Follette, K. B., Rameau, J., Dong, R., et al. 2017, AJ, 153, 264, doi: 10.3847/1538-3881/aa6d85

Gaia Collaboration, Brown, A. G. A., Vallenari, A., et al. 2018, ArXiv e-prints. https://arxiv.org/abs/1804.09365

Gressel, O., Nelson, R. P., Turner, N. J., & Ziegler, U. 2013, ApJ, 779, 59, doi: 10.1088/0004-637X/779/1/59

Hord, B., Lyra, W., Flock, M., Turner, N. J., & Mac Low, M.-M. 2017, ApJ, 849, 164, doi: 10.3847/1538-4357/aa8fcf

Isella, A., Chandler, C. J., Carpenter, J. M., Pérez, L. M., & Ricci, L. 2014, ApJ, 788, 129, doi: 10.1088/0004-637X/788/2/129

Keppler, M., Benisty, M., Müller, A., et al. 2018, A&A, 617, A44, doi: 10.1051/0004-6361/201832957

Keppler, M., Teague, R., Bae, J., et al. 2019, arXiv e-prints, arXiv:1902.07639. https://arxiv.org/abs/1902.07639

Kraus, A. L., & Ireland, M. J. 2012, ApJ, 745, 5, doi: 10.1088/0004-637X/745/1/5

Ligi, R., Vigan, A., Gratton, R., et al. 2018, MNRAS, 473, 1774, doi: 10.1093/mnras/stx2318

Lubow, S. H., Seibert, M., & Artymowicz, P. 1999, ApJ, 526, 1001, doi: 10.1086/308045

McMullin, J. P., Waters, B., Schiebel, D., Young, W., & Golap, K. 2007, in Astronomical Society of the Pacific Conference Series, Vol. 376, Astronomical Data Analysis Software and Systems XVI, ed. R. A. Shaw, F. Hill, & D. J. Bell, 127

Mendigutía, I., Oudmaijer, R. D., Schneider, P. C., et al. 2018, A&A, 618, L9, doi: 10.1051/0004-6361/201834233

Miki, S. 1982, Progress of Theoretical Physics, 67, 1053, doi: 10.1143/PTP.67.1053

Pavlov, A., Feldt, M., & Henning, T. 2008, in Astronomical Society of the Pacific Conference Series, Vol. 394, Astronomical Data Analysis Software and Systems XVII, ed. R. W. Argyle, P. S. Bunclark, & J. R. Lewis, 581

Pérez, S., Casassus, S., & Benítez-Llambay, P. 2018, MNRAS, 480, L12, doi: 10.1093/mnrasl/sly109

Perez, S., Dunhill, A., Casassus, S., et al. 2015, ApJ, 811, L5, doi: 10.1088/2041-8205/811/1/L5

Pineda, J. E., Szulágyi, J., Quanz, S. P., et al. 2019, ApJ, 871, 48, doi: 10.3847/1538-4357/aaf389

Pinte, C., Price, D. J., Ménard, F., et al. 2018, ApJ, 860, L13, doi: 10.3847/2041-8213/aac6dc

Price, D. J., Cuello, N., Pinte, C., et al. 2018, MNRAS, 477, 1270, doi: 10.1093/mnras/sty647

Quanz, S. P., Amara, A., Meyer, M. R., et al. 2015, ApJ, 807, 64, doi: 10.1088/0004-637X/807/1/64

—. 2013a, ApJ, 766, L1, doi: 10.1088/2041-8205/766/1/L1

Quanz, S. P., Avenhaus, H., Buenzli, E., et al. 2013b, ApJ, 766, L2, doi: 10.1088/2041-8205/766/1/L2

Rameau, J., Follette, K. B., Pueyo, L., et al. 2017, AJ, 153, 244, doi: 10.3847/1538-3881/aa6cae

Reggiani, M., Quanz, S. P., Meyer, M. R., et al. 2014, ApJ, 792, L23, doi: 10.1088/2041-8205/792/1/L23

Reggiani, M., Christiaens, V., Absil, O., et al. 2018, A&A, 611, A74, doi: 10.1051/0004-6361/201732016

Ricci, L., Cazzoletti, P., Czekala, I., et al. 2017, AJ, 154, 24, doi: 10.3847/1538-3881/aa78a0

Sallum, S., Follette, K. B., Eisner, J. A., et al. 2015, Nature, 527, 342, doi: 10.1038/nature15761

Simpson, J. M., Smail, I., Swinbank, A. M., et al. 2015, ApJ, 799, 81, doi: 10.1088/0004-637X/799/1/81

Sissa, E., Gratton, R., Garufi, A., et al. 2018, A&A, 619, A160, doi: 10.1051/0004-6361/201732332

Szulágyi, J., Morbidelli, A., Crida, A., & Masset, F. 2014, ApJ, 782, 65, doi: 10.1088/0004-637X/782/2/65

Thalmann, C., Janson, M., Garufi, A., et al. 2016, ApJ, 828, L17, doi: 10.3847/2041-8205/828/2/L17

Thiébaut, E. 2008, in Society of Photo-Optical Instrumentation Engineers (SPIE) Conference Series, Vol. 7013, Optical and Infrared Interferometry, 70131I

Wu, Y.-L., Close, L. M., Eisner, J. A., & Sheehan, P. D. 2017, AJ, 154, 234, doi: 10.3847/1538-3881/aa93db

Zhu, Z., Andrews, S. M., & Isella, A. 2018, MNRAS, 479, 1850, doi: 10.1093/mnras/sty1503